DOI: 10.31276/VJSTE.2024.0056

Numerical investigation of the collision of a vortex ring with a wavy sphere

Nguyen Van Luc[1, 2*], Le Tuan Phuong Nam[3], Phan Toai Tuyn[4]

[1]Division of Computational Mechanics, Institute for Advanced Study in Technology, Ton Duc Thang University, 19 Nguyen Huu Tho Street, Tan Phong Ward, District 7, Ho Chi Minh City, Vietnam
[2]Faculty of Civil Engineering, Ton Duc Thang University, 19 Nguyen Huu Tho Street, Tan Phong Ward, District 7, Ho Chi Minh City, Vietnam
[3]Institute of Engineering and Technology, Thu Dau Mot University, 6 Tran Van On Street, Phu Hoa Ward, Thu Dau Mot City, Binh Duong Province, Vietnam
[4]Institute for Computational Science and Technology, SBI Building, Quang Trung Software City, Tan Chanh Hiep Ward, District 12, Ho Chi Minh City, Vietnam

Received 28 May 2024; revised 17 June 2024; accepted 29 July 2024

Abstract:

The numerical investigation of vortex dynamics resulting from the collision of a vortex ring with a wavy sphere of various wavenumbers (n) at a Reynolds number of 1000 was conducted using a developed remeshed vortex particle method. The influence of the wall's wavenumber on vortex dynamic mechanisms, such as the primary vortex ring's deformation, the boundary layer's separation, and the formation, interaction, and reconnection of secondary and tertiary vortices, was analysed. When the primary ring collides with a smooth sphere (n=0), secondary and tertiary rings are formed, and their interaction with the primary ring is similar to that observed with a flat plate. In the case of the wavy sphere, the boundary layer separates from the wall's hills more rapidly than from the valleys, leading to the boundary layer rolling up into the secondary vortex in a wavy pattern. The segments of the secondary vortex originating from the hills move around the primary ring, while those from the valleys convect upwards, forming incomplete vortex loops at n=5. However, at n=9, the reconnection of segments from the valleys results in the formation of a chain of small-scale rings. Furthermore, tertiary vortices are generated from the valleys due to the additional separation of the wall boundary layer induced by the secondary vortex segments in the valleys. These vortices dissipate rapidly at n=5, whereas reconnection occurs to form additional vortex loops at n=9.

Keywords: **fluid dynamics, vortex dynamics, vortex interactions.**

Classification numbers: **2.1, 2.3**

1. Introduction

Vortex-wall interaction is widely observed in engineering applications as well as natural processes, such as wingtip vortices near the ground in aerospace engineering, the conning tower of submarines in naval engineering, computer chips mounted on electrical circuit boards in the electronics industry, and flow around buildings in civil engineering [1]. A comprehensive understanding of this flow phenomenon is essential for improving the design and control of related devices. Consequently, this has attracted the interest of many numerical and experimental researchers over several decades. The vortex ring has frequently been employed to examine the characteristics of vortex-wall interaction because it has a simple prototype structure and is relatively easy to produce. However, it can cause various flow phenomena when colliding with a wall. When a vortex ring moves towards a wall, it induces a boundary layer on the wall. The wall geometry strongly influences this boundary layer's distribution, intensity, and separation. These characteristics lead to different phenomena of vortex dynamics (formation, deformation, merging, breakdown, and reconnection) when a distinctive wall geometry is applied.

The wall geometries often employed to investigate vortex flow, vortex instability, and vortex interaction include flat plates [2, 3], V-walls [4], round cylinders [5], and spheres [6, 7]. When a vortex ring collides with a flat wall at a low Reynolds number (Re), the ring dissipates without generating a secondary vortex ring. At a moderate Re and some low angles of incidence of the wall, the collision produces a secondary vortex ring, or even a tertiary one [2]. This secondary ring develops azimuthal instability and may even form hairpin-like small vortices. As the angle of incidence increases beyond a critical value, depending on the Reynolds number, the primary vortex ring generates only the secondary ring, which then evolves into a helical structure [3]. When a vortex ring collides

*Corresponding author: Email: nguyenvanluc@tdtu.edu.vn

with a V-wall, leapfrogging of the secondary and tertiary rings past the primary ring occurs. The upstream separated boundary layers interact with these rings to produce small daisy-chained vortex dipoles [4]. T.H. New, et al. (2017) [5] reported that the behaviour of the collision of a vortex ring on a round cylinder differs from that on a flat plate, in which the disconnection and reconnection of the primary and secondary vortex rings produce small-scale vortex ringlets. These vortex ringlets may even collide to form vortex dipoles further. These vortex ringlets even collide to form vortex dipoles further. V.L Nguyen, et al. (2019) [6] pointed out that when a vortex ring collides coaxially with a sphere, the deformation of the primary ring and its interaction with the secondary and tertiary rings are similar to the flat plate, and the collision is two-dimensional. However, the non-coaxial collision of a vortex ring with a sphere forms a three-dimensional vortex without the formation of a secondary vortex ring. T.H. New, et al. (2024) [7] further explained the recurring formation of the tertiary vortex ring due to the slowdown of the primary vortex ring. This slowdown leads to the entrainment of the tertiary ring into the primary ring and renders it incoherent. The primary ring then continues to induce another tertiary ring. The primary ring then continues to induce another tertiary ring.

Some specific wall geometries have also been explored due to their potential engineering applications and to extend the fundamental knowledge of vortex dynamics. T. Ahmed, et al. (2023) [8] investigated the collision of a vortex ring with a hemispherical cavity and found loop-like instabilities in the secondary vortex ring. Moreover, another ring is formed on the lip/edge of the cavity, and this ring disrupts the separation of the wall-bounded boundary layer, which forms the secondary ring. H. Ren, et al. (2014) [9] employed a large-eddy simulation to study the collision of a vortex ring with a bump at a Reynolds number of 4×10^4. They discovered that the bump height greatly influences the induced vortex shapes and turbulent flow. They also revealed that wrapping and hairpin vortices are vital in the flow's transition from laminar to turbulent. Wrapping vortices are related to azimuthal instability in the vortex rings, whereas the primary vortex ring causes the hairpin vortex formation. These hairpin vortices impinge on the bump's surface, breaking into smaller ones. H. Ren, et al. (2015) [10] discovered that when a thin or thick vortex ring collides with a flat wall, the large-scale wrapping and hairpin vortices break down into smaller ones. This breakdown obeys the - 5/3 power law, suggesting a fully developed turbulent flow. Moreover, they also found that thin and thick vortex rings suffer from instabilities with modes of 11 and 16, respectively. M. Cheng, et al. (2014) [11] numerically investigated the impact of a three-dimensional vortex ring on a permeable wall for a range of physical and flow parameters, including wall open-area ratio, structural dimension, wall thickness, and Reynolds number. They found that these parameters affect flow characteristics upstream and downstream of a permeable wall. Increasing the wall open-area ratio or Reynolds number improves vorticity transport over the porous wall, resulting in a regenerated vortex ring. Conversely, increasing wall thickness hinders vorticity transport and the development of regenerated vortex rings. A. Pirnia, et al. (2017) [12] investigated the vortex dynamics and flow-induced vibrations of a flexible plate arising from a vortex ring passing tangentially over it. When the centreline of the vortex ring is positioned greater than approximately twice the vortex ring radii away from the plate, it can be considered as the far field, and the resulting vibrations are well predicted through the potential flow model. As the offset distance of the vortex ring decreases, the diffusion of induced vorticity on the plate into the flow field significantly alters the fluid dynamics, pressure loading, and resultant plate dynamics, dramatically increasing the strain energy compared to the potential flow model.

Previous research has provided fundamental knowledge on vortex dynamics resulting from the collision of a vortex ring with a solid wall. However, a comprehensive understanding of vortex dynamics has not yet been elucidated, and expanding the scope of knowledge on flow dynamics remains of interest. It is clear that vortex dynamics depend strongly on the geometry of the solid wall, and several solid wall models with potential applications in heat transfer engineering have yet to be examined. In this study, we will focus on clarifying the characteristics of the vortex dynamics caused by the collision of a vortex ring with a wavy sphere of various wavenumbers. To our knowledge, prior researchers have not yet conducted flow dynamics investigations with this type of wall. We will demonstrate that the mechanisms of vortex dynamics, such as vortex formation, interaction, and reconnection, induced by the collision of a vortex ring with a solid wavy sphere, strongly depend on the wall's wavenumber. The remainder of this article is organised as follows: the numerical method and its validation are discussed in Section 2, the simulation results are analysed in Section 3, and the conclusions are presented in Section 4.

2. Numerical method and its validation

The mass and momentum Navier-Stokes equations for the flow of an incompressible viscous fluid around a solid body are written in the velocity-pressure form as:

$$\nabla \cdot \boldsymbol{u} = 0 \tag{1}$$

$$\frac{\partial \boldsymbol{u}}{\partial t} + (\boldsymbol{u} \cdot \nabla)\boldsymbol{u} = -\frac{1}{\rho}\nabla p + \upsilon \nabla^2 \boldsymbol{u} + \boldsymbol{g} + \lambda(\boldsymbol{u} - \boldsymbol{u}_S) \tag{2}$$

where ∇ is the gradient operator; $\frac{\partial \boldsymbol{u}}{\partial t}$ is the derivative of $\boldsymbol{u}$ with respect to t, t is the time; $\boldsymbol{u}$ is flow velocity; p is pressure; $\rho$is the fluid density; υ is the kinematic viscosity of the fluid;

∇^2 is the Laplace operator; $\boldsymbol{g}$ is gravitational acceleration; $\boldsymbol{u}_S$ is solid velocity; and λ is penalisation parameter. The last term in Eq. (2) expresses the appearance of the solid body in fluid flow, where the no-slip condition of flow is imposed on this body surface using the penalisation technique. When taking the curl operation on both sides of Eq. (2), the momentum equation is expressed in the velocity - vorticity form as

$$\frac{\partial \boldsymbol{\omega}}{\partial t} + (\boldsymbol{u}\cdot\nabla)\boldsymbol{\omega} = (\boldsymbol{\omega}\cdot\nabla)\boldsymbol{u} + \upsilon\nabla^2\boldsymbol{\omega} + \nabla\times\left[\lambda(\boldsymbol{u}-\boldsymbol{u}_S)\right] \quad (3)$$

where the vorticity is defined as $\boldsymbol{\omega} = \nabla\times\boldsymbol{u}$. The fluid is discretized into vortex particles p at position $\boldsymbol{x}_p$ carrying the vorticity field $\boldsymbol{\omega}(x_p)$ with the flow velocity $\boldsymbol{u}(\boldsymbol{x}_p)$. Therefore, the transport momentum equation, Eq. (2), can be rewritten in the Lagrangian reference frame of vortex particles p as

$$\frac{d\boldsymbol{x}_p}{dt} = \boldsymbol{u}(\boldsymbol{x}_p) \quad (4)$$

$$\frac{d\boldsymbol{\omega}(\boldsymbol{x}_p)}{dt} = \left[\boldsymbol{\omega}(\boldsymbol{x}_p)\cdot\nabla\right]\boldsymbol{u}(\boldsymbol{x}_p) + \upsilon\nabla^2\boldsymbol{\omega}(\boldsymbol{x}_p) + \nabla\times\left[\lambda\left(\boldsymbol{u}(\boldsymbol{x}_p)-\boldsymbol{u}_S(\boldsymbol{x}_p)\right)\right] \quad (5)$$

The vorticity field of the vortex particles is updated on the grid using Eq. (5). These particles move at their velocity $\boldsymbol{u}(\boldsymbol{x}_p)$ using Eq. (4). Their velocity on the grid is calculated using the stream function $\boldsymbol{\psi}$ as $\boldsymbol{u} = \nabla\times\boldsymbol{\psi}$, while $\boldsymbol{\psi}$ is computed using the Poisson equation, $\nabla^2\boldsymbol{\psi} = -\boldsymbol{\omega}$. The numerical method described above is known as a remeshed-vortex particle method. A further explanation of the current numerical method is found in the previous research by V.L. Nguyen, et al. (2021) [13].

The current numerical method is verified using the benchmark problem of the collision of a vortex ring upon a flat solid wall at the Reynolds number of Re_Γ = 1743, where the ring at the outset is modelled using a Gaussian distribution function as

$$(\omega_r, \omega_\theta, \omega_z) = \left(0, \frac{\Gamma}{\pi\sigma^2} e^{-\frac{r^2(x,y,z)}{\sigma^2}}, 0\right) \quad (6)$$

where $r^2(x,y,z) = \left(r_0 - \sqrt{(x-x_0)^2 + (y-y_0)^2}\right)^2 + (z-z_0)^2$, (x_0, y_0, z_0)=(0,0,3r_0) is the initial position of the vortex ring, r_0=1 is the ring radius, and σ=0.21r_0 is the initial core radius. The Reynolds number of the vortex ring is defined as Re_Γ=Γ/ν, where Γ=1 is the initial ring circulation. The distance between the ring and the plane surface at the outset is set as 3r_0. The computational domain of (–4r_0, 4r_0)×(–4r_0, 4r_0)×(–2r_0, 6r_0) is discretized into 320^3 cubic grid cells, and the time step (Δt^*=$\Delta t\Gamma/r_0^2$) is set as 0.002. Using the r_0 and Γ, the flow quantities are rewritten in the nondimensional form as follows: $\boldsymbol{x}^*$=x/r_0, t^*=t/Γr_0^2, $\boldsymbol{u}^*$=$\boldsymbol{u}r_0/\Gamma$, $\boldsymbol{\omega}^*$=$\boldsymbol{\omega}r_0^2/\Gamma$, ω_y^*=$\omega_y r_0^2/\Gamma$. The total enstrophy and kinetic energy are respectively defined as

$$Ens(t^*) = \frac{1}{2}\int_V \boldsymbol{\omega}^{*2}(\boldsymbol{x}^*, t^*)dV \quad (7)$$

$$Ek(t^*) = \frac{1}{2}\int_V \boldsymbol{u}^{*2}(\boldsymbol{x}^*, t^*)dV \quad (8)$$

where V indicates the whole computational domain.

Figure 1 shows the time evolution of the collision of a vortex ring with a flat plane at Re_Γ = 1743. The creation of the boundary layer and the secondary ring, their interaction with the primary ring, and the primary ring's rebound phenomenon are visible. From the figure, the present simulation results agree well with the experimental ones provided by C.C. Chu, et al. (1993) [2]. Fig. 2 describes the time variation of the primary vortex ring center. The primary ring's rebound phenomenon develops due to the secondary ring pushing it upward. The current simulation results also agree with the experimental data [2]. Thus, the present numerical method adequately captures the vortex dynamics induced by the collision of a vortex with a solid wall.

Figure 3 shows the time variation of the total enstrophy and kinetic energy of the flow caused by the collision of a vortex ring with a flat plate at Re_Γ=1743 using four grid resolutions. The total enstrophy of the flow slightly reduces from the outset to t^*=8 due to vortex diffusion effects. This diffusion spreads the vorticity field to neighbouring locations, but it reduces the overall intensity of vorticity. The total enstrophy dramatically increases from t^*=8 to 16 because of the formation of the boundary layer as the primary ring approaches the wall. The enstrophy is maximal at t^*=16 when the secondary vortex ring is formed. During the final stage of the flow, the total enstrophy strongly decreases because the diffusion of existing vortices plays a vital role in the flow. The total kinetic energy of the flow slightly reduces in the early stage of the flow from the beginning to t^*=12 before a drastic decrease for the remaining period. This is explained by dissipation happening throughout the flow period, and its rate is faster after the secondary vortex ring is formed. From the figure, we observe that the results of total enstrophy are convergent as the grid resolution increases, and the difference in enstrophy between two resolutions using 280^3 and 320^3 grid cells is insignificant. The results of the total kinetic energy of the flow almost overlap as the grid resolution varies. Therefore, we will use the grid resolution of 320^3 grid cells for later simulations.

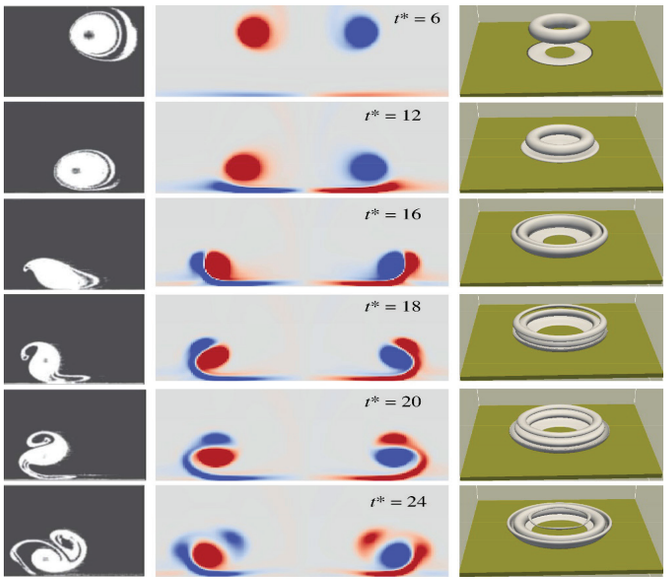

Fig. 1. Time evolution of the vortex structures induced by the collision of a vortex ring upon a flat plane at Re_Γ= 1743. The first column is experimental data given by C.C. Chu, et al. (1993) [2]. The second and third columns present simulation results plotted using the vorticity contour of ω_y^* on the x-z plane and the vorticity magnitude $|\omega^*|$=1.

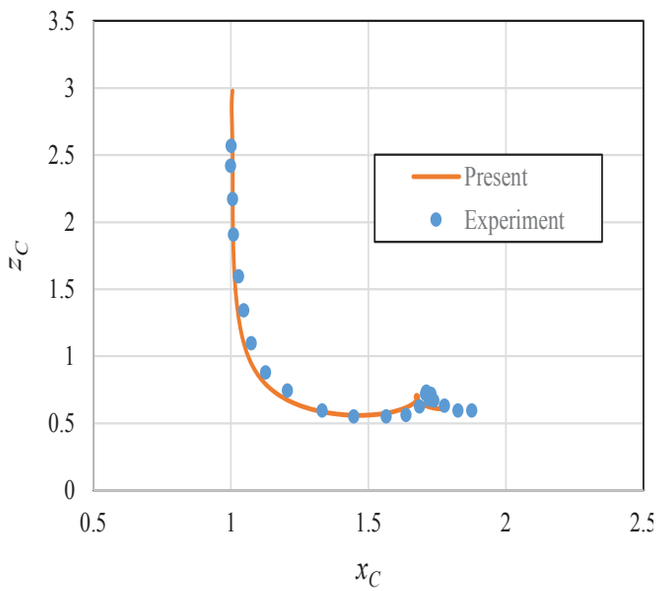

Fig. 2. Time variation of the primary vortex ring centre (x_c, z_c). The current simulation results are compared with the experimental results given by C.C. Chu, et al. (1993) [2].

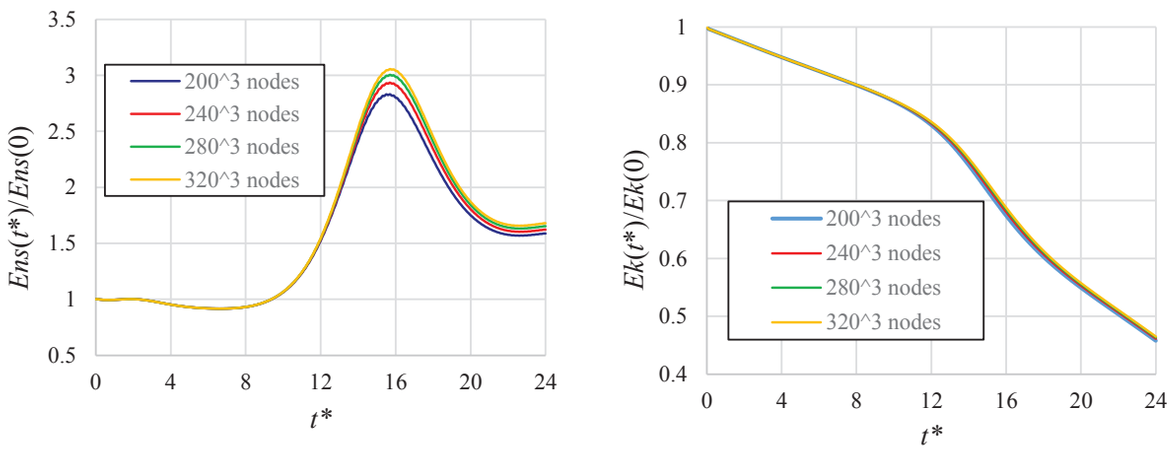

Fig. 3. Time evolution of the total enstrophy (*Ens*) and total kinetic energy (*Ek*) of the flow induced by the collision of a vortex ring with a flat plate at Re_Γ=1743.

3. Results and discussion

The collision of a vortex ring with a wavy sphere is numerically investigated at Re_Γ =1000, where the vortex ring at the outset is modelled using the Gaussian distribution function, as described above. The vortex ring has a radius of $r_0 = 1$, core radius of $\sigma = 0.21 r_0$ at the position of (0, 0, $4r_0$). The wavy sphere surface is modelled as

$$\frac{x^2 + y^2}{\left(R + a\sin\left(n\theta\right)\right)^2} + \frac{z^2}{R^2} = 1 \qquad (9)$$

where R=$2r_0$; n = 0, 5, 9 is the wavenumber; a=$0.05r_0$ is the wave amplitude; and $\theta = \sin^{-1}\left(y / \sqrt{x^2 + y^2}\right)$. The computational domain is set as ($-4r_0$, $4r_0$) × ($-4r_0$, $4r_0$) × ($-4r_0$, $6r_0$). The grid resolution and the time step are the same as those used for the above simulation of the collision of a vortex ring on a flat plane.

Figures 4 and 5 show the time evolution of the collision of a vortex ring upon a sphere (n=0) at Re_Γ =1000, where the vortex structures are expressed using plots of the vorticity contour and the iso-surface of Q-criteria, with the colour range from blue to red representing the enstrophy values from -1 to 1. The boundary layer is generated on the sphere surface as the primary vortex ring moves toward the sphere at t^*=2 and 4. This boundary layer separates from the sphere surface at t^*=6 and rolls up to form the secondary vortex ring at t^*=8. This vortex moves around the primary vortex ring while the boundary layer separates from the sphere at t^*=10. The shear layer rolls up to create the tertiary vortex ring at t^*=12. During the last stage of the flow, the secondary and tertiary vortex rings gradually decay with time, and they disappear at t^*=20. The behaviour of the primary ring, the formation of the secondary ring, and their interaction are similar to those observed in the case of a flat wall.

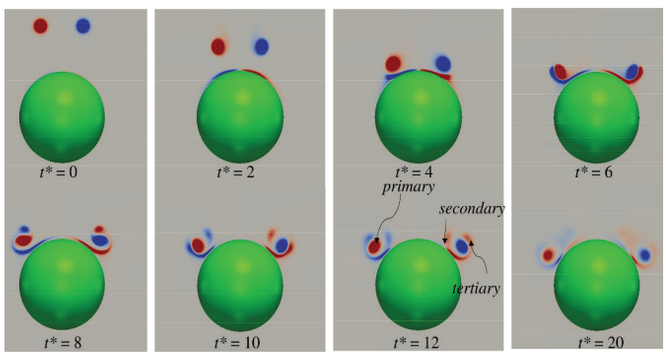

Fig. 4. Time evolution of the collision of a vortex ring upon a sphere with n=0 at Re_Γ= 1000, in which the vortex structures are represented using the vorticity contour of ω_y^* on the *x-z* plane.

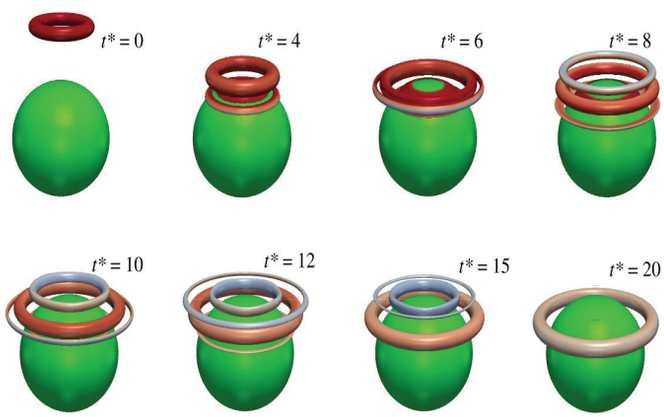

Fig. 5. Time evolution of the collision of a vortex ring upon a sphere with n=0 at Re_Γ=1000, where the vortex structures are represented using the iso-surface of Q-criteria and the

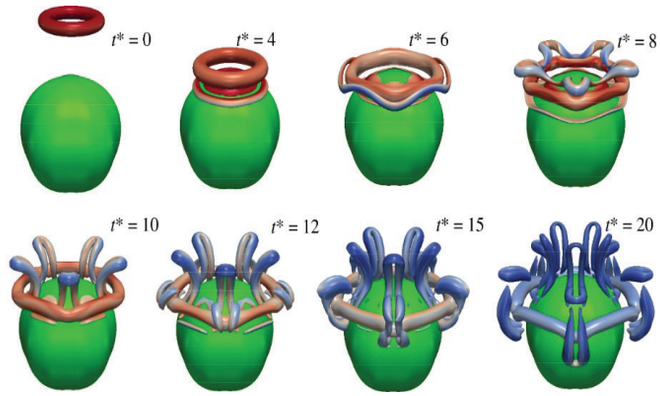

Fig. 6. Time evolution of the collision of a vortex ring upon a wavy sphere with n=5 at Re_Γ=1000, where the vortex structures are represented using the iso-surface of Q-criteria and the enstrophy.

Figure 6 describes the time variation of the collision of a vortex ring with a wavy sphere with n=5 at Re_Γ=1000, in which the vortex structures are represented using the iso-surface Q-criteria with the colour range representing the enstrophy. The boundary layer is also formed as the vortex ring advances closer to the wall, as seen at t^*=4. The boundary layer on the hills (the peaks of the wave) first separates from the wall, followed by that at the valleys (the bottoms of the wave), and they roll up to produce the secondary vortex at t^*=6. The portion of the secondary vortex near the hills moves around the primary vortex at t^*=8, while the rest of the secondary vortex ring remains behind. At this moment, the boundary layer continues to separate from the wall. During the last stage of the flow, the secondary vortex near the hills decays, while that near the valleys rises upward into incomplete vortex loops. Furthermore, the tertiary vortices generated at the valleys move around the primary vortex, as shown at t^*=15 and 20. The primary vortex is significantly deformed due to its interaction with the secondary and tertiary vortices. The reconnection of the secondary and tertiary vortices is incomplete before they dissipate over time.

Figure 7 illustrates the time evolution of the vortex structures induced by the collision of a vortex ring with a wavy sphere at n=9 and Re_Γ=1000. We observe that the boundary layer first separates at the hills and subsequently at the valleys, leading to the formation of the secondary vortex at t^*=6. The portion of this vortex originating from the wall hills rapidly moves around the primary vortex, while the part from the valleys ascends at t^*=8. At this stage, the boundary

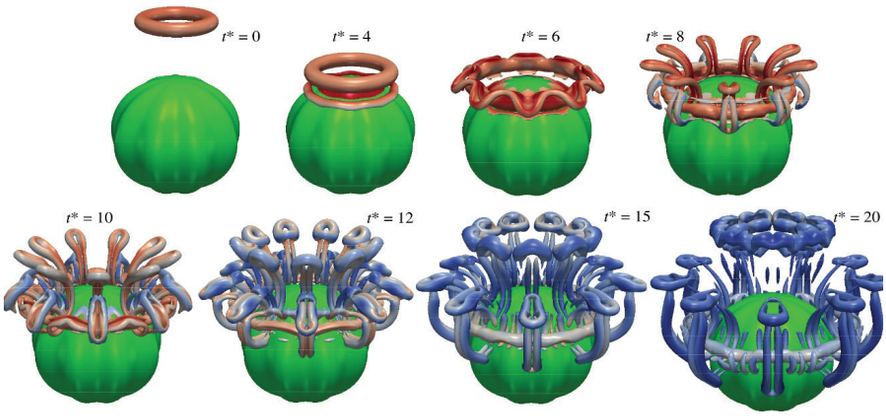

Fig. 7. Time evolution of the collision of a vortex ring upon a wavy sphere with n=9 at Re_Γ = 1000, where the vortex structures are represented using the iso-surface of Q-criteria and the enstrophy.

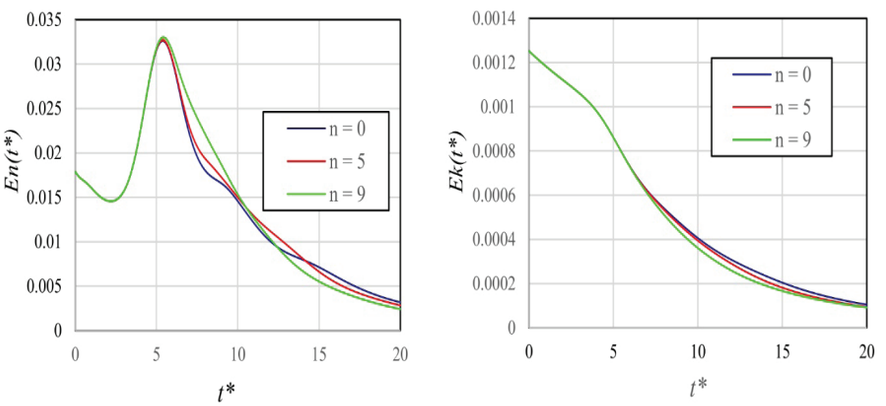

Fig. 8. Time evolution of the total enstrophy (*En(t*)*) and kinetic energy (*Ek(t*)*) of the flow induced by the collision of a vortex ring with a wavy sphere at Re_Γ=1000, where n stands for number of wavelengths.

layer separates from the wall, forming tertiary vortex loops. By t^*=10, the part of the secondary vortex detached from the hills deforms the primary vortex significantly, while the remainder from the valleys reconnects, forming small-scale vortex rings that ascend. A portion of the secondary vortex continues to move around the primary vortex at t^*=12 before decaying at t^*=15 and 20. In contrast to the scenario with n=5, the reconnection of the secondary vortex that separated from the valleys is more complete, resulting in a chain of smaller vortex rings. Additionally, the tertiary vortex from the valleys successfully reconnects, producing vortex loops. These findings indicate that the reconnection of the secondary and tertiary vortices occurs over a greater number of wavelengths.

Figure 8 illustrates the temporal evolution of the total enstrophy and kinetic energy of the flow induced by the collision of a vortex ring with a wavy sphere at various wavelengths. The total enstrophy gradually decreases during the initial stages of the flow as the vortex ring diffuses. Enstrophy then increases significantly between t^*=2.5 due to the formation of a boundary layer on the wall as the ring approaches, which generates a vorticity field near the wall. After t∗=5, enstrophy decreases sharply as the boundary layer formation completes, and the diffusion of the primary and secondary vortices becomes prominent during the final stages of the flow. The peaks of the wave cause a higher enstrophy throughout the interval t^*=5. There is a slight change in enstrophy at t^*=10 as the boundary layer separates, leading to the formation of tertiary vortices. In the concluding phase of the flow, from t^*=14, the enstrophy for the wavy wall with a higher number of peaks is reduced, which is attributed to the wavy wall dissipating vortices at a greater rate compared to a smooth wall.

4. Conclusions

Numerical simulations of the collision of a vortex ring with a wavy sphere at various wavenumbers (n) and Re_Γ=1000 are performed for the first time using the vortex particle method. The numerical method is validated against the benchmark simulation of a vortex ring impinging on a flat plate at Re_Γ=1743. The simulation results indicate that the current numerical method successfully captures the vortex dynamics induced by the collision of a vortex with a solid wall. The key findings for the collision of a vortex ring with a wavy sphere are summarised as follows:

When a vortex ring collides with a smooth sphere (n=0), secondary and tertiary vortex rings are formed due to the separation and rolling up of the boundary layer on the wall. Their interaction with the primary vortex ring is similar to

that observed in the flat plate case, where they move around the primary ring, resulting in the rebound phenomenon, before dissipating over time. The difference here is the tendency for the boundary layer to separate more easily from the sphere than from the flat plate.

For the collision of a vortex ring with a wavy wall, the behaviour of the secondary and tertiary vortices is highly dependent on the wavenumber (n) of the wall. The boundary layer on the hills (wave crests) separates first, followed by the valleys (wave troughs), leading to the formation of a secondary vortex ring in a wavy pattern. This vortex near the hills moves around the primary vortex ring, while the remainder near the valleys ascends. At n=9, these parts reconnect to form small-scale vortex rings, whereas at n=5, the reconnection does not occur, resulting in incomplete vortex loops. Tertiary vortices are generated in the valleys as the secondary vortex ring ascends. These vortices also reconnect to form vortex loops at n=9, while reconnection does not take place at n=5.

CRediT author statement

Nguyen Van Luc: Algorithm, Simulation, Original draft preparation, Reviewing, Editing; Le Tuan Phuong Nam, Phan Toai Tuyn: Simulation, Writing, Reviewing, and Editing.

ACKNOWLEDGEMENTS

This research is funded by the Vietnam National Foundation for Science and Technology Development (NAFOSTED) under grant number 107.03-2021.27.

COMPETING INTERESTS

The authors declare that there is no conflict of interest regarding the publication of this article.

REFERENCES

[1] T.L. Doligalski, C.R. Smith, J.D.A. Walker (1994), "Vortex interactions with walls", *Annual Review of Fluid Mechanics*, **26(1)**, pp.573-616, DOI: 10.1146/annurev.fl.26.010194.003041.

[2] C.C. Chu, C.T. Wang, C.S. Hsieh (1993), "An experimental investigation of vortex motions near surfaces", *Physics of Fluids A*, **5(3)**, pp.662-676, DOI: 10.1063/1.858650.

[3] M. Cheng, J. Lou, L.S. Luo (2010), "Numerical study of a vortex ring impacting a flat wall", *J. Fluid Mech.*, **660**, pp.430-455, DOI: 10.1017/S0022112010002727.

[4] T.H. New, J. Long, B. Zang, et al. (2020), "Collision of vortex rings upon V-walls", *Journal of Fluid Mechanics*, **899**, DOI: 10.1017/jfm.2020.425.

[5] T.H. New, B. Zang (2017), "Head-on collisions of vortex rings upon round cylinders", *Journal of Fluid Mechanics*, **833**, pp.648-676, DOI: 10.1017/jfm.2017.599.

[6] V. L. Nguyen, K. Takamure, T. Uchiyama (2019), "Deformation of a vortex ring caused by its impingement on a sphere", *Physics of Fluids*, **31(10)**, DOI: 10.1063/1.5122260.

[7] T.H. New, B. Xu, S. Shi (2024), "Collisions of vortex rings with hemispheres", *Journal of Fluid Mechanics*, **980**, DOI: 10.1017/jfm.2024.13.

[8] T. Ahmed, B.D. Erath (2023), "Experimental study of vortex ring impingement on concave hemispherical cavities", *Journal of Fluid Mechanics*, **967**, DOI: 10.1017/jfm.2023.501.

[9] H. Ren, C. Xu (2014), "Three-dimensional numerical simulation of a vortex ring impacting a bump", *Theoretical and Applied Mechanics Letters*, **4(3)**, DOI: 10.1063/2.1403204.

[10] H. Ren, X.Y. Lu (2015), "Dynamics and instability of a vortex ring impinging on a wall", *Communications in Computational Physics*, **18(4)**, pp.1122-1146, DOI: 10.4208/cicp.150115.210715s.

[11] M. Cheng, J. Lou, T.T. Lim (2014), "A numerical study of a vortex ring impacting a permeable wall", *Physics of Fluids*, **26(10)**, DOI: 10.1063/1.4897519.

[12] A. Pirnia, J. Hu, S.D. Peterson, et al. (2017), "Vortex dynamics and flow-induced vibrations arising from a vortex ring passing tangentially over a flexible plate", *Journal of Applied Physics*, **122(16)**, DOI: 10.1063/1.5009068.

[13] V.L. Nguyen, H.L. Duong, N.T.P. Le (2021), "Oblique collision and reconnection of a vortex ring with a vortex tube", *Physics of Fluids*, **33(12)**, DOI: 10.1063/5.0073126.